Diode and fibre pumped Cr^{2+}:ZnS mid-infrared external cavity and microchip lasers

S.B. Mirov, V.V. Fedorov, K. Graham, I.S. Moskalev, I.T. Sorokina, E. Sorokin, V. Gapontsev, D. Gapontsev, V.V. Badikov and V. Panyutin

Abstract: Demonstrations of CW and pulsed microchip lasing in Cr^{2+}:ZnS and Cr^{2+}:ZnSe crystals are reported. Slope efficiencies up to 53% with output power up to 150 mW for CW and energy up to 1 mJ for pulsed pumping were achieved. Two compact diode and Er fibre laser directly pumped external cavity Cr^{2+}: ZnS lasers are also described.

1 Introduction

There is a growing demand for affordable, compact, room temperature and broadly tunable mid-infrared (IR) laser sources for use in a variety of applications. DeLoach *et al.* [1] and Page *et al.* [2] have recently performed detailed spectroscopic studies of several II–VI chalcogenide hosts with different divalent transition metal ions (TM^{2+}) as potential mid-IR laser materials. These pioneering publications [1, 2] introduced to the laser community a new class of mid-IR laser media and explained why TM^{2+}:II–VI compounds are so special for mid-IR lasing. TM (Cr^{2+}, Co^{2+}, V^{2+}, Mn^{2+}, Fe^{2+}, Ni^{2+}) doped II–VI (II = Cd, Zn; VI = S, Se, Te) compounds have a wide band gap and possess three important features that distinguish them from other oxide and fluoride laser crystals:

(*a*) The existence of chemically stable divalent TM dopant ions, which substitute for Zn^{2+} or Cd^{2+} host ions, with no need for charge compensation.
(*b*) The tendency to crystallise as tetrahedrally coordinated structures, as opposed to the typical octahedral coordination at the dopant site. Tetrahedral coordination (T_d) gives smaller crystal field splitting, placing the dopant transitions further into the IR.
(*c*) Finally, a key feature of these materials is the low energy of optical phonon cut-off that decreases the efficiency of non-radiative decay and gives promise of a high yield of fluorescence at room temperature.

Since then, this class of lasers has attracted a lot of attention and laser demonstrations over the 2–3 μm spectral region in CW, free-running long pulse, Q-switched and mode-locked regimes of operation were reported for Cr:ZnS [3, 4], Cr:ZnSe [5–9], Cr : $Cd_{1-x}Mn_xTe$ [10] and Cr:CdSe [11] crystals.

Active interest in TM doped II–VI compounds is explained by the fact that these media are close mid-IR analogues of titanium-doped sapphire (Ti–S) in terms of spectroscopic and laser characteristics, and it is anticipated that TM^{2+} doped chalcogenides will lase with a great variety of possible regimes of oscillation, similar to the Ti–S laser. Hence, TM^{2+} doped II–VI materials feature excellent laser properties in the mid-IR, as well as showing promise for their use in a variety of applications, such as environmental analysis, remote sensing, spectroscopy and medicine. Among this class of lasers the most impressive results have been obtained so far using Cr^{2+}:ZnSe crystals [5–9]. Cr^{2+}:ZnS has not been extensively studied as a laser material, perhaps due to the lack of good optical quality single crystals. Having spectroscopic properties similar to Cr^{2+}:ZnSe, Cr^{2+}:ZnS is known to have a larger band gap (3.84 versus 2.83 eV [12]), better mechanical properties and lower dn/dT ($+46 \times 10^{-6}$ versus $+70 \times 10^{-6}/°C$ [1]). Therefore, the power handling capability of this material should be higher, making Cr^{2+}:ZnS attractive for high power applications.

In this study we extend our efforts to develop high optical density and high quality Cr^{2+}:ZnS and Cr^{2+}:ZnSe crystals synthesised by chemical transport reaction from the gas phase and activated by the diffusion doping, additive colouration method [3, 4]. Other key objectives of this research have been to provide the first demonstration of CW lasing of Cr^{2+}:ZnS crystals under direct fibre and diode laser excitation, and specifically investigate the feasibility of Cr^{2+}:ZnS and Cr^{2+}:ZnSe crystals lasing in a microchip configuration under CW Er-fibre laser pumping. These microchip lasers are important candidates for cost effective and compact lasers since they have a very short cavity length from a few hundred μm up to a few mm [13].

2 Crystal preparation

Bulk Cr^{2+}:ZnS crystals can be obtained from melt [14] or vapour growth techniques [14] by including the dopant in the starting charge. Under atmospheric pressure ZnS is sublimed at a temperature higher than about 1180 °C before melting [15]. Therefore for melt growth, in addition to high temperature (1950 °C), it is necessary to apply high

IEE Proceedings online no. 20030612

doi: 10.1049/ip-opt:20030612

Paper first received 31st October 2002 and in revised form 31st March 2003

S.B. Mirov, V.V. Fedorov, K. Graham and I.S. Moskalev are with the Department of Physics, The University of Alabama at Birmingham, 1300 University Boulevard, Birmingham, AL 35244-1170, USA

I.T. Sorokina and E. Sorokin are with the Institut für Photonik, TU Wien, Gusshausstrasse, 27/387, A-1040 Vienna, Austria

V. Gapontsev and D. Gapontsev are with the IPG Photonics Corporation, 50 Old Webster Road, Oxford, MA 01540, USA

V.V. Badikov and V. Panyutin are with the Kuban State University, 149 Stavropolskaya Street, Krasnodar, 350040, Russia

pressure, up to 75×10^5 Pa [15]. This inconvenience of the high temperature melt growth of ZnS might be accompanied by uncontrolled contamination inducing undesired absorptions. On the other hand, the control of the amount of Cr^{2+} ions incorporated in the crystal is difficult using vapour growth techniques [16, 17]. Hence, in addition to Cr^{2+}:ZnS samples grown by the physical vapour transport (PVT) method, thermally activated after-growth diffusion of Cr in ZnS was also utilised in this work as an alternative.

After-growth doped Cr^{2+}:ZnS crystals were prepared by a two-stage method. During the first stage, undoped single crystals were synthesised by a chemical vapour transport (CVT) reaction from the gas phase using an iodine gas transport scheme in a quartz tube of 20 mm diameter and 200 mm length placed in a two-zone furnace. At the second stage, chromium was introduced into the crystalline host by thermal diffusion carried out in sealed ampoules under a pressure of 10^{-5} torr and a temperature of 1000 °C over 5–20 days. Some crystals, at the second stage of chromium introduction into the crystalline host, were doped by thermal diffusion from a chromium thin film deposited by a pulse laser deposition method on a thin wafer of II–VI material.

X-ray analysis revealed hexagonal matrices in both crystals with the following lattice constants: $a = b = 0.381$ nm, $c = 0.935$ nm, $\alpha = \beta = 90°$, $\gamma = 120°$. However, the structure of the crystals was not that of wurtzite but was a modification of the cubic structure, with a certain degree of hexagonality. Such crystals are known to demonstrate natural birefringence. The lowering of the local crystalline field symmetry as a result of anisotropy may cause an increase in the oscillator strength and a corresponding decrease in the lifetime. Indeed, our luminescence and lifetime measurements produced a larger transition cross-section and shorter room-temperature lifetime than reported earlier for cubic Cr:ZnS crystals (16×10^{19} cm^{-2} and 5.7 μs, respectively, versus 7.5×10^{19} cm^{-2} and 8 μs in [1]).

3 Spectroscopic characterisation

The room-temperature absorption and fluorescence spectra of the Cr^{2+}:ZnS and Cr^{2+}:ZnSe crystals are given in cross-section units in Figs. 1*a* and 1*c*, respectively. The absorption spectra were measured using a Shimadzu UV-VIS-NIR-3101PC spectrophotometer. The fluorescence spectra were measured using an Acton Research ARC-300i spectrometer and a liquid nitrogen cooled EGG Judson J10D-M204-R04M-60 InSb detector coupled to a Perry PA050 amplifier. This InSb detector–amplifier combination featured a temporal resolution of 0.4 μs. The fluorescence spectra were corrected with respect to the spectral sensitivity of the recording system using an Oriel 9-2050 tungsten halogen calibration lamp. As an excitation source we used a CW erbium doped fibre laser (IPG Group ELD-2), modulated at 800 Hz. It is noteworthy that Cr^{2+}:ZnSe crystals did not exhibit any polarisation dependence of the absorption and the difference due to the polarisation dependence of the absorption and fluorescence spectra for Cr:ZnS did not exceed 10% at room temperature. This allowed us to treat the crystal, to a first approximation, as optically isotropic.

The luminescence kinetics of the crystals were measured at 1950, 2100, 2400 and 2600 nm across a broad temperature range using D_2 and H_2 Raman-shifted Nd:YAG laser excitation at 1560 and 1907 nm. Within the 0.4 μs accuracy of measurements there was no difference in the lifetime of luminescence for different wavelengths of excitation and registration. Figure 1*b* shows that the emission lifetime drops only slightly for ZnS, i.e. from 5.7 to 4.3 μs, between 14 and 300 K and is practically unchanged for ZnSe (Fig. 1*d*). This shows that quenching is not important below 300 K. Further heating of the ZnS crystal leads to a drastic decrease of the lifetime, which at 450 K was already below the detector time constant.

The spontaneous-emission cross-sections $\sigma_{em}(\lambda)$ (Figs. 1*a* and 1*c*) were obtained from the fluorescence intensity signal $I(\lambda)$ using the Fuchtbauer–Ladenburg equation:

$$\sigma_{em}(\lambda) = \frac{\lambda^5 I_\lambda(\lambda) A}{8\pi n^2 c \int I_\lambda(\lambda)\lambda d\lambda} \quad (1)$$

where A is the spontaneous emission probability from the upper laser level, and n is the index of refraction.

To derive the absorption cross-section magnitude from the absorption spectrum, one needs to know the Cr^{2+} concentration. Unfortunately, the absolute dopant concentration is neither uniform nor accurately known in the case of diffusion doping. We therefore used the reciprocity method for the broadband transition:

$$\sigma_a(\lambda) = \sigma_{em}(\lambda)\frac{Z_2}{Z_1}\exp\left(\frac{(hc/\lambda) - E_{ZFL}}{kT}\right) \quad (2)$$

in conjunction with measured absorption spectra to calculate the absorption cross-section in Figs. 1*a* and 1*c*, making use of the known upper and ground level partition functions ratio $z_2/z_1 = 0.66$. Here E_{ZFL} is the energy of the zero phonon line of the corresponding transition measured in [3, 4] from the low-temperature fluorescence spectra, k is the Boltzmann constant, and T is the temperature. Our value for the peak absorption cross-section of $\sigma_a = 1.6 \times 10^{-18}$ cm^2 at $\lambda = 1690$ nm for Cr^{2+}:ZnS [18] agrees reasonably well with the value of $\sigma_a = 1.0 \times 10^{-18}$ cm^2 obtained using the absorption coefficient and the known concentration of Cr^{2+} in [19].

4 Er fibre laser pumped Cr^{2+}:ZnS and Cr^{2+}:ZnSe CW microchip lasers

Microchip laser experiments on both Cr^{2+}:ZnS and Cr^{2+}:ZnSe CVT grown crystals were performed and reported in [20–22]. The crystals were polished flat and parallel (parallelism of ~10 arcsec) to 1.0 and 2.5 mm thickness, respectively. The mirrors were directly deposited on the parallel polished facets of a thin wafer of laser material. The input and output dichroic mirrors had 0.01 and 3.5% transmission over the 2300–2500 nm spectral region, respectively. Two different pump arrangements were utilised. The first was identical to the pump conditions for Cr^{2+}:ZnS CW lasing in a hemispherical cavity [20, 21]. The second pump arrangement had no coupling optics, and the microchip laser was mounted at a close (~20 μm) distance from the tip of the Er-fibre pump laser. Figure 2 shows the output power of the Cr^{2+}:ZnS and Cr^{2+}:ZnSe microchip lasers plotted as a function of absorbed pump power.

In a focused pump beam arrangement a laser threshold of 120 mW and a slope efficiency of 53% with respect to the absorbed pump power were achieved for the Cr^{2+}:ZnS microchip laser. The high slope efficiency of the microchip laser, close to the theoretical limit of 65%, indicates that the crystal is of high quality with low loss. The maximum output power reached 58 mW and was limited by a relatively small amount of active optical centres. When the microchip was scanned with respect to the laser beam it was found that there are zones in the crystal with a twice as large absorption coefficient of the Cr^{2+} and slightly larger losses. For these regions that appear to be near the edges of

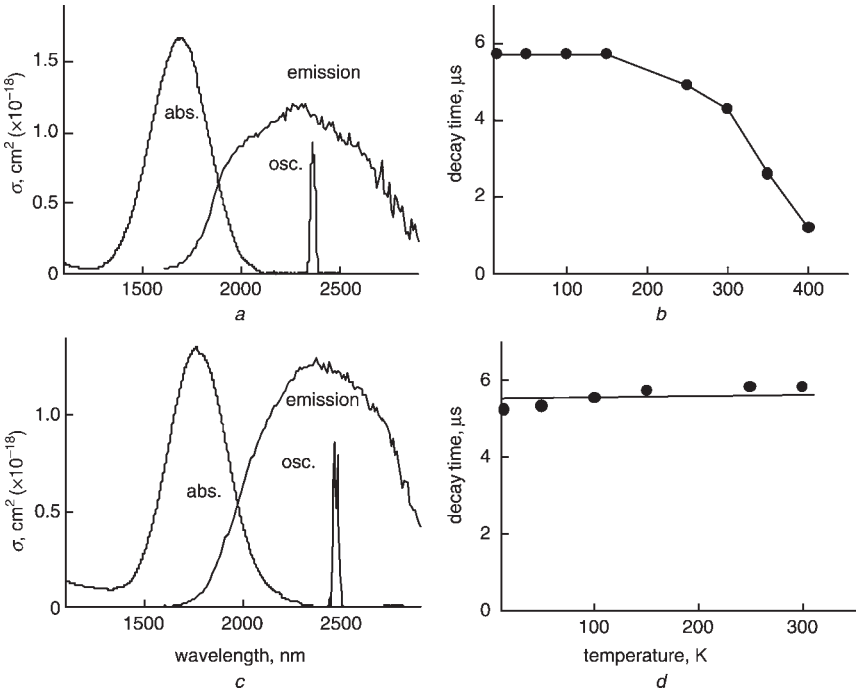

Fig. 1 *Spectroscopic characterisation of Cr^{2+}:ZnS and Cr^{2+}:ZnSe*

a Room-temperature cross-section of absorption, emission and oscillation spectra of Cr^{2+}:ZnS
b Temperature dependence of luminescence lifetime of Cr^{2+}:ZnS
c Room-temperature cross-section of absorption, emission and oscillation spectra of Cr^{2+}:ZnSe
d Temperature dependence of luminescence lifetime of Cr^{2+}:ZnSe

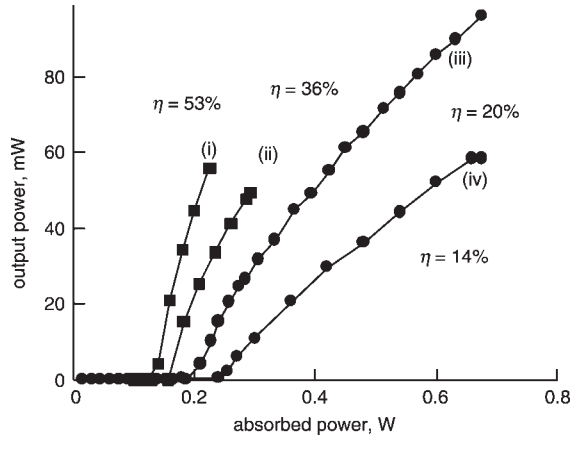

Fig. 2 *Output–input characteristics of the Cr^{2+}:ZnS [(i), (ii)] and Cr^{2+}:ZnSe [(iii), (iv)] continuous wave microchip lasers under Er-fibre laser excitation*

(i), (iii) Focused pump beam arrangement
(ii), (iv) No coupling optics between the fibre tip and the microchip

the microchip the maximum output power of the Cr^{2+}: ZnS microchip laser reached 150 mW at a slope efficiency of 43%.

Thermal effects provided cavity stabilisation within the microchip crystals and were responsible for the slightly non-linear character of the output versus input laser performance. For ZnSe microchip lasing with a focused pump beam arrangement, a laser threshold of 190 mW, a slope efficiency of 20% with respect to the absorbed pump power, and a maximum output power of 100 mW were demonstrated. The doubled output power of Cr:ZnSe with respect to Cr:ZnS can be explained by the twice as large optical density of the ZnSe microchip.

In the second pump arrangement, when the microchip lasers were directly coupled to the fibre tip, laser thresholds of 150 mW and 240 mW and slope efficiencies of 36 and 14% with respect to absorbed pump power were achieved for Cr^{2+}:ZnS and Cr^{2+}:ZnSe microchip lasers, respectively. The maximum output power of the Cr^{2+}:ZnS microchip laser was virtually unchanged in either pump arrangement, however it dropped, for Cr^{2+}:ZnSe, by a factor of 1.6 when the crystal was directly coupled to the fibre tip compared to the focused pump arrangement. This can be explained by the excessive length and corresponding mismatch of the mode size and pump beam profile of the ZnSe microchip.

The output spectra in free-running laser operation covered the 2280–2350 nm and 2550–2620 nm spectral ranges for the ZnS and ZnSe microchip lasers, respectively. At maximum pump power the output spectrum of the Cr^{2+}:ZnSe laser consisted of more than 100 axial modes with a free spectral range $\Delta\nu = 0.8\,cm^{-1}$. The typical output spectra of the microchip lasers are depicted in the traces labelled (i) in Fig. 3. Due to the smaller crystal thickness, the free spectral range of the Cr^{2+}:ZnS microchip laser was $\Delta\nu = 2\,cm^{-1}$ and the output spectrum consisted of about 50 axial modes. We attempted to arrange mode control of the microchip lasers by means of a coupled cavity arrangement, with an additional external mirror. The coupled microchip and mirror produced the spectral structure shown in the traces labelled (ii) in Fig. 3. In these experiments the number of axial modes decreased to 18–24 modes (each line in traces (ii) of Fig. 3 consists of three longitudinal modes) for both lasers. This can be further decreased to a single longitudinal mode oscillation in a coupled cavity configuration using a narrowband output coupler, as was successfully demonstrated for Tm:YLF by Izawa *et al.* [23].

Figure 4 depicts the far field divergence pattern of the Cr^{2+}:ZnS and Cr^{2+}:ZnSe microchip lasers. As one can see, a 20 mrad full width at half maximum (FWHM) of the intensity profile was measured for the Cr^{2+}:ZnS laser. This is slightly less than that for the Cr^{2+}:ZnSe laser (25 mrad).

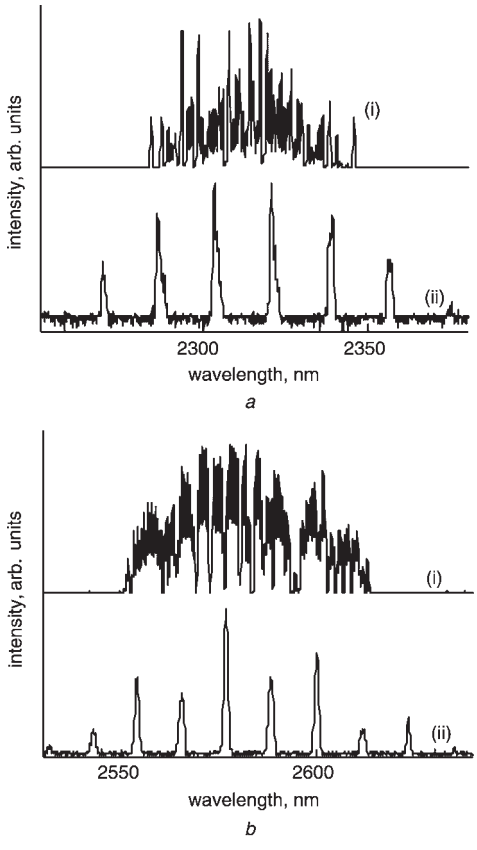

Fig. 3 *Spectral output of Cr^{2+}: ZnS and Cr^{2+}: ZnSe microchip lasers and coupled cavity microchip lasers*

(i) Microchip lasers; (ii) coupled cavity microchip lasers
a Cr^{2+}:ZnS
b Cr^{2+}:ZnSe

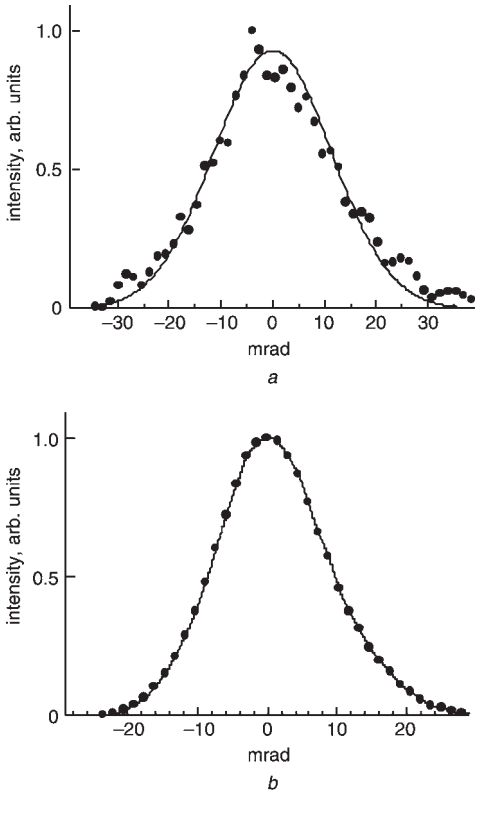

Fig. 4 *Far-field spatial distribution of output radiation of Cr^{2+}:ZnS and Cr^{2+}: ZnSe microchip lasers*

a Cr^{2+}:ZnS
b Cr^{2+}:ZnSe

Taking thermal effects, which are responsible for cavity stabilisation, into account, the divergence difference may be explained by a lower dn/dT in the Cr^{2+}:ZnS crystal ($+46 \times 10^{-6}\,K^{-1}$ in ZnS versus $+70 \times 10^{-6}\,K^{-1}$ in ZnSe).

5 Gain switched Cr^{2+}:ZnS and Cr^{2+}:ZnSe microchip lasers

Gain switched microchip laser experiments were performed with CVT grown ZnS and ZnSe crystals; however, the best results were obtained with ZnSe [22]. The ZnSe crystal used was 5.5 mm thick with polished but uncoated parallel faces and had a coefficient of absorption of $k = 6\,cm^{-1}$ at 1.77 μm. Pumping was via the 1.56 μm output of a D_2 Raman shifted Nd:YAG laser operating at 10 Hz with a pulse duration of about 5 ns and 1.5 mm beam diameter. Output–input energies for pulsed ZnSe microchip lasing for different lasing spots are shown in Fig. 5. Threshold input energy was found to be 7 mJ. A maximum slope efficiency of 6% with respect to pump energy and maximum output energy of 1 mJ were obtained. The spectral range of the free-running laser output was from 2270 to 2290 nm.

6 Er fibre and diode laser pumped continuous wave tunable Cr^{2+}:ZnS lasers [18, 24]

The laser cavity, shown in Fig. 6*a*, was formed by a flat dichroic mirror, a folding mirror with an $R = 50$ mm radius of curvature, and a plane output coupler varying from 1% to 10%. The plane-parallel crystalline plate was mounted on the room-temperature aluminium holder. The crystal of the PVT-grown Cr:ZnS was a ~2.5-mm-thick uncoated plate with 98% absorption at 1.6 μm. For comparison, we used a 1-mm-thick antireflection-coated CVT-grown Cr:ZnS sample (60% absorption at 1.6 mm). The diode-pumped Er-fibre laser (IPG Laser, 5 W polarised output) was focused on to the crystal by the uncoated 75-mm lens. Alternatively, we used two InGaAsP-InP laser diodes, each providing up to 0.5 W of the output power from a 100-μm broad stripe (Fig. 6*b*). Approximately 55% of the available pump power was actually absorbed in the crystal: 34% was lost in the collimating system, and 15% was due to the reflection on the uncoated ZnS crystal surface.

To explore the limits of Cr:ZnS crystals in terms of power and tunability, we first used the Er-fibre laser as a pump source. With a 10% output coupler, the output power reached 700 mW at 2.65 W of absorbed pump power, with a 110-mW threshold (filled circles, Fig. 7*a*). The excessive

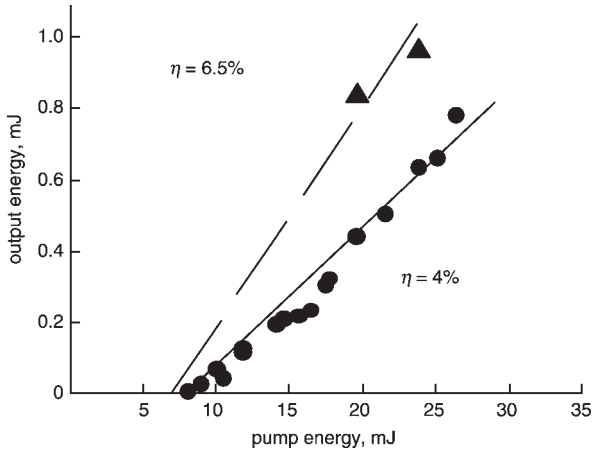

Fig. 5 *Output–input characteristics of gain-switched Cr^{2+}: ZnSe microchip laser*

▲ and ● represent different crystal spots

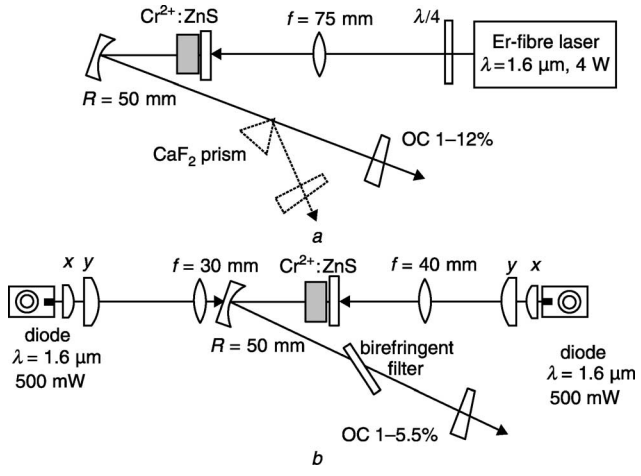

Fig. 6 *Schematic diagrams of tunable Cr^{2+}:ZnS laser setup*

a Er-fibre laser pumped setup
b Diode-pumped setup

thermal loading prevented pumping of the laser much over 2.65 W of absorbed power. The physical mechanisms of the roll-off could be the thermal self-focusing of the pump, thermal lensing, or lifetime thermal quenching. However, using a 1:1 chopper, we could achieve more than 1 W of output power (open circles, Fig. 7*a*) at 34% slope efficiency. This result correlates with the 40% slope efficiency found in the case of the CVT-grown sample (triangles, Fig. 7*a*), which had slightly lower losses per round trip (5.5 ± 0.5% versus 7 ± 1.5%), measured with the inverse slope efficiency analysis [25]. This analysis also gave a value of 63% as the limiting slope efficiency, which is close to the 68% quantum limit at 2350 nm.

Using a CaF_2 Brewster prism as a tuning element, we were able to demonstrate tunability over ~700 nm from 2170 to 2840 nm (filled circles, Fig. 7*b*), using a single mirror set. Using the shorter-wavelength optics, we could extend the tuning range down to 2110 nm (open circles, Fig. 7*b*). We believe that extension of the tuning range toward the infrared is also feasible with the use of a corresponding set of mirrors and purging of the resonator to remove water vapour (grey curve in Fig. 8*b*). The oscillation linewidth was measured to be less than 0.4 nm and was limited by the resolution of our monochromator.

Direct diode-pumped operation was acheived with two pump diodes simultaneously, as shown in Fig. 6*b*). The laser output characteristics in the case of the diode pumping of Cr:ZnS are given in Fig. 8. The threshold power of the Cr:ZnS laser was 175 mW of absorbed power. With a 6.8% output coupler, the polarised TEM00 laser output reached 25 mW at 570 mW of absorbed power and a slope efficiency of ~8%. We were also able to demonstrate diode-pumped operation of the CVT-grown Cr:ZnS crystal, but because of the low absorption and pump reflection on the crystal surfaces, the

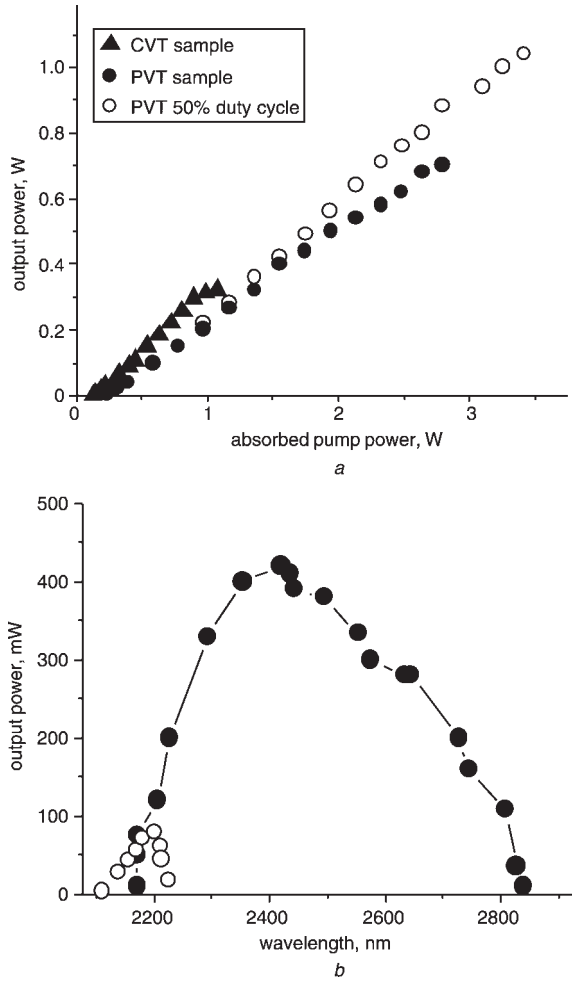

Fig. 7 *Power and tuning of Cr:ZnS*

a Output characteristics of different Cr : ZnS samples under Er-fibre laser pumping and 10% output coupling
b Tuning of the PVT sample under Er-fibre laser pumping. The filled and open circles refer to different mirror sets, centred at 2400 and 2100 nm, respectively

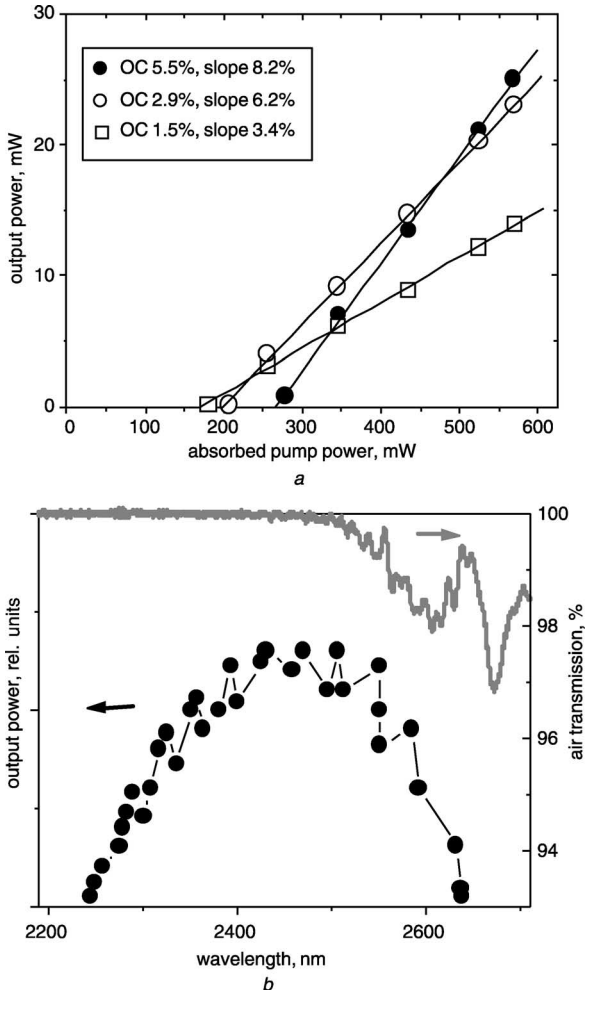

Fig. 8 *Characteristics of Cr:ZnS laser under diode pumping*

a Output characteristics of Cr : ZnS laser (PVT sample) under diode pumping
b Tuning curve of PVT Cr : ZnS under diode pumping. The grey curve shows air transmission, normalised to the resonator length

maximum output power was only 1.1 mW. Using a birefringent (Lyot) filter made from crystalline quartz as a tuning element, we could demonstrate smooth tunability over 400 nm, from 2250 to 2650 nm (Fig. 8*b*). To our knowledge, this tuning range is the broadest ever demonstrated in the diode-pumped chalcogenides. Under the same conditions, the tuning range of the Cr:ZnSe sample was limited to 350 nm [9]. This difference results from the blue shift of the Cr:ZnS emission band relative to Cr:ZnSe. On the red side, the tuning range of both crystals is limited by the water vapour absorption in the resonator [9]. Since Cr:ZnS can be tuned further into the short-wavelength side, its usable tuning range is broader. The fine structure of the tuning curves is due to the etalon effect of the air gap between the crystal surface and the input mirror. The oscillation linewidth was measured to be less than 0.4 nm. Since the spectral luminescent parameters of the Cr:ZnS sample are close to those of Cr:ZnSe, we explain the lower efficiency and higher threshold of Cr:ZnS by the higher (factor of 3–4) passive losses. This means that improvement in the crystal growth and diffusion-doping techniques of Cr:ZnS should lead to improvement of the laser parameters up to at least the level of Cr:ZnSe, with the advantage of lower dn/dT as well as a larger band gap. The latter decreases the probability of multiphoton absorption at high intensity.

7 Conclusions

In conclusion, laser characterisation of diffusion doped Cr^{2+}:ZnS and Cr^{2+}:ZnSe crystals synthesised by chemical transport reaction from the gas phase and by the physical transport method were studied under CW Er-doped fibre laser and direct diode laser excitation. To our knowledge this is the first successful demonstration of a CW Cr^{2+}:ZnS microchip laser with maximum output power of 150 mW at 2320, and slope efficiency of 53% under direct Er-fibre laser excitation.

The first gain switched Cr^{2+}:ZnSe microchip laser was demonstrated with a maximum slope efficiency of 6.5% and maximum output energy of 1 mJ. These results were obtained for a microchip without mirrors, when positive feedback was due only to Fresnel reflections.

The first demonstration of a directly tunable diode-pumped CW Cr^{2+}:ZnS laser, pumped by two conventional 500 mW InGaAsP-InP telecom laser diodes has been reported. Tunability over 400 nm between 2250 and 2650 nm was achieved.

Finally, in an external cavity configuration a compact Er-fibre laser pumped, CW room-temperature Cr^{2+}:ZnS laser, broadly tunable over ~700 nm between 2100 and 2840 nm, was built, yielding up to 700 mW at ~40% slope efficiency.

Further optimisation of these lasers will certainly stimulate a number of new applications such as field-portable spectroscopy systems for scientific, commercial, medical and military applications.

8 Acknowledgments

The authors thank Dr. Kathleen Schaffers for providing the PVD grown Cr^{2+}:ZnS crystals used in this work.

9 References

1 DeLoach, L.D., Page, R.H., Wilke, G.D., Payne, S.A., and Krupke, W.F.: 'Transition metal-doped zinc chalcogenides: spectroscopy and laser demonstration of a new class of gain media', *IEEE J. Quantum Electron*, 1996, **32**, pp. 885–895

2 Page, R.H., Schaffers, K.I., DeLoach, L.D., Wilke, G.D., Patel, F.D., Tassano, J.B., Payne, S.A., Krupke, W.F., Chen, K.T., and Burger, A.: 'Cr^{2+}-doped zinc chalcogenides as efficient, widely tunable mid-infrared lasers', *IEEE J. Quantum Electron*, 1997, **33/4**, pp. 609–619

3 Graham, K., Mirov, S.B., Fedorov, V.V., Zvanut, M.E., Avanesov, A., Badikov, V., Ignat'ev, B., Panutin, V., and Shevirdyaeva, G.: 'Spectroscopic characterization and laser performance of diffusion doped Cr^{2+}:ZnS', in Payne, S., and Marshall, C. (Eds.): 'Advanced solid state lasers', vol. 46 of OSA Proceedings Series (Optical Society of America, Washington DC, 2001), pp. 561–567

4 Graham, K., Mirov, S., Fedorov, V., Zvanut, M.E., Avanesov, A., Badikov, V., Ignat'ev, B., Panutin, V., and Shevirdyaeva, G.: 'Laser performance of Cr^{2+} doped-ZnS', *Proc. SPIE -Int. Soc. Opt. Eng.*, 2001, **4267**, pp. 81–88

5 Wagner, G.J., Carrig, T.J., Page, R.H., Schaffers, K.I., Ndap, J.O., Ma, X., and Burger, A.: 'Continuous-wave broadly tunable Cr^{2+}:ZnSe laser', *Opt. Lett.*, 1999, **24**, pp. 19–21

6 Carrig, T.J., Wagner, G.J., Sennaroglu, A., Jeong, J.Y., and Pollock, C.R.: 'Acousto-optic mode-locking of a Cr^{2+}:ZnSe laser', in Injeyan, H., Keller, U., and Marshall, C. (Eds.): 'Advanced solid state lasers', vol. 34 of OSA Proceedings Series (Optical Society of America, Washington DC, 2001), pp. 182–187

7 Podlipensky, A.V., Shcherbitsky, V.G., Kuleshov, N.V., Levchenko, V.I., Yakimovich, V.N., Mond, M., Heumann, E., Huber, G., Kretschmann, H., and Kuck, S.: 'Efficient laser operation and continuous-wave diode pumping of Cr^{2+}:ZnSe single crystals', *Appl. Phys. B, Lasers Opt.*, 2001, **72**, pp. 253–255

8 Sorokin, E., Sorokina, I.T., and Page, R.H., 'Room-temperature CW diode-pumped Cr^{2+}:ZnSe laser', in Payne, S., and Marshall, C. (Eds.): 'Advanced solid state lasers', vol. 46 of OSA Proceedings Series (Optical Society of America, Washington DC, 2001), pp. 101–105

9 Sorokin, E., and Sorokina, I.T.: 'Tunable diode-pumped continuous-wave Cr^{2+}:ZnSe laser', *Appl. Phys. Lett.*, 2002, **80**, pp. 3289–3291

10 Hommerich, U., Wu, X., Davis, V.R., Trivedi, S.B., Grasza, K., Chen, R.J., and Kutcher, S.: 'Demonstration of room-temperature laser action at 2.5 μm from Cr^{2+} : $Cd_{0.85}Mn_{0.15}Te$', *Opt. Lett.*, 1997, **22**, pp. 1180–1182

11 McKay, J., Kraus, D., and Schepler, K.L.: 'Optimization of Cr^{2+}: CdSe for efficient laser operation', in Injeyan, H., Keller, U., and Marshall, C., (Eds.): 'Advanced solid state lasers', vol. 34 of OSA Proceedings Series (Optical Society of America, Washington DC, 2001), pp. 218–224

12 Segall, B., and Marple, D.T.F.: in Aven, M., and Prener, J.S. (Eds.): 'Physics and Chemistry of II–IV compounds' (North Holland, Amsterdam, 1967), pp. 319–381

13 Zayhowski, J.J., and Mooradian, A.: 'Single-frequency microchip Nd lasers', *Opt. Lett.*, 1989, **14**, pp. 24–26

14 Kukimoto, H., Shionoya, S., Koda, T., and Hioki, R.: 'Infrared absorption due to donor states in ZnS crystals', *J. Phys. Chem. Solids*, 1968, **29**, pp. 935–940

15 Vij, D.R., and Singh, N.: 'Luminescence and related properties of II–VI semiconductors' (Nova Science Publishers, Inc, Commack, NY, 1998)

16 Su, C.-H., Feth, S., Voltz, M.P., Matyi, R., George, M.A., Chattopadhyay, K., Burger, A., and Lehoczky, S.L.: 'Vapour growth and characterization of Cr-doped ZnSe crystals', *J. Cryst. Growth*, 1999, **207**, pp. 35–42

17 Ndap, J.-O., Chattopadhyay, K., Adetunji, O.O., Zelmon, D.E., and Burger, A.: 'Thermal diffusion of Cr^{2+} in bulk ZnSe', *J. Cryst. Growth*, 2002, **240**, pp. 176–184

18 Sorokina, I.T., Sorokin, E., Mirov, S., Fedorov, V., Badikov, V., Panyutin, V., Di Lieto, A., and Tonelli, M.: 'Continuous-wave tunable Cr^{2+} : ZnS laser', *Appl. Phys. B, Lasers Opt.*, 2002, **74**, pp. 607–611

19 Kelley, C.S., and Williams, F.: 'Optical absorption spectra of chromium-doped zinc-sulfide crystals', *Phys. Rev. B*, 1970, **2**, pp. 3–8

20 Mirov, S.B., Fedorov, V.V., Graham, K., Moskalev, I.S., Badikov, V.V., and Panutin, V.: 'Mid-IR and ZnSe microchip lasers', in Fermann, M.E., and Marshall, L.R. (Eds.): 'Advanced solid state lasers', (Optical Society of America, Washington DC, 2002), pp. 364–370

21 Mirov, S.B., Fedorov, V.V., Graham, K., Moskalev, I., Badikov, V., and Panyutin, V.: 'Er-fibre laser pumped continuous-wave microchip Cr^{2+}: ZnS and Cr^{2+}: ZnSe lasers', *Opt. Lett.*, 2002, **27**, pp. 909–911

22 Mirov, S.B., Fedorov, V.V., Graham, K., Moskalev, I.S., Badikov, V.V., and Panutin, V.: 'CW and pulsed Cr^{2+}:ZnS and ZnSe microchip lasers', in 'OSA Trends in Optics and Photonics (TOPS) vol. 73, Conference on Lasers and Electro-Optics', OSA Technical Digest, Postconference edn., (Optical Society of America, Washington DC, 2002), pp. 120–121

23 Izawa, J., Nakajima, H., Hara, H., and Arimoto, Y.: 'A tunable and longitudinal mode oscillation of a Tm, Ho:YLF microchip laser using an external etalon', *Opt. Commun.*, 2000, **180**, pp. 137–140

24 Sorokina, I.T., Sorokin, E., Mirov, S.B., Fedorov, V.V., Badikov, V., Panyutin, V., and Schaffers, K.: 'Broadly tunable compact continuous-wave Cr^{2+} : laser', *Opt. Lett.*, 2002, **27**, pp. 1040–1042

25 Caird, J.A., Payne, S.A., Staver, P.R., Ramponi, A.J., Chase, L.L., and Krupke, W.F.: 'Quantum electronic properties of the $Na_3Ga_2Li_3F_{12}$: Cr^{3+} laser', *IEEE J. Quantum Electron*, 1988, **24**, pp. 1077–1099